Accepted Manuscript
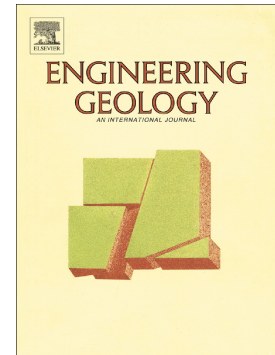
Structure-based hydro-mechanical properties of sand-bentonite composites

Soheil Ghadr, Arya Assadi-Langroudi

Please cite this article as: Soheil Ghadr, Arya Assadi-Langroudi , Structure-based hydro-mechanical properties of sand-bentonite composites. The address for the corresponding author was captured as affiliation for all authors. Please check if appropriate. Engeo(2018), doi:10.1016/j.enggeo.2018.02.002

Structure-based Hydro-Mechanical Properties of Sand-bentonite Composites

GHADR, Soheil [First and Corresponding Author]

Eastern Mediterranean University

Address: İsmet İnönü Bulvarı, Gazimağusa, Famagusta, Northern Cyprus [1]

Email: soheil.ghadr25@gmail.com

Tel: +98 914 340 9081

ASSADI-LANGROUDI, Arya [Second Author]

School of Architecture, Computing & Engineering, University of East London

Email: a.assadilangroudi@uel.ac.uk

Tel: +44 8223 2170

---

[1] Current (Permanent) Address: Faculty of Engineering, Urmia State University, Sero Rd., Urmia, Iran, 5756151818

Abstract

For the geological disposal of highly contaminated wastes, medical or other sorts, clay barrier systems are commonly designed and used. The engineered liners contain buffer material which is often carefully proportioned mixtures of pure bentonite and sand. Bentonite is an active clay mineral with very low hydraulic conductivity and extremely high expansive properties, which benefits in controlling the downward migration of hazardous contaminants to groundwater. In the design of such composite buffer geomaterial, deformation and pore-flow analysis is a pivotal matter and has therefore been thoroughly investigated in the decades past. When unsaturated, the coupling hydraulic-mechanical behaviour of sand-bentonite mixtures are complex. Among possible reasons behind this complex behaviour is the dependency of hydraulic hysteresis and consolidation properties on size, shape and sorting of solids and pores in the soil's skeleton, which are also rarely accounted for in most of the commonly used soil models.

In this contribution, the hydro-mechanical behaviour of saturated and unsaturated sand-bentonite soil is investigated in the context of the recently developed *Concept of Double Porosity (CDP).* The geomaterial under study is assumed to consist of an incompressible, rigid, elastic solid skeleton surrounded by viscous water and gas fluids, and connected via a network of elastoplastic clayey bridge/buttress units. *Roundness* and *sorting* are varied for the sand constituent. The *clay fraction (CF)* is also varied across testing specimens. The experimental work here introduces two micromechanical models (small clay and large clay) which facilitates interpretation of macro-scale coupled hydromechanical behaviour of composite sand-bentonite geomaterials. The findings from this work will aid design practitioners through a tentative decision support system proposed in closing remarks.

Keywords: Sand-bentonite, hydro mechanical, microstructure, suction, liner.

1. Introduction

Bentonite belongs to the expansive smectite clay minerals, and is commercially available from modification of volcano ash. High swelling capacity and low hydraulic conductivity of bentonite makes it suitable for use as a sealing material in buffers around buried wastes and liners in landfills (Kaoser et al. 2006). Bentonite's low permeability is hoped to constrain the efflux of contaminants into the groundwater system. Nevertheless, Bentonite's high swelling pressure, is a risk to the encapsulated containers; making sand-bentonite mixtures an attractive alternative buffer material (Wersin et al. 2007). Compacted sand-bentonite mixtures (through dynamic or static compression – cf. Ito and Komin, 2008) are commonly used as buffer constituent of landfill barrier systems owing to their good resistance to imposed thermal gradients, low likelihood of structural damage on freeze-thaw, and limited shrinkage-related volume change on cyclic wetting and drying (Kraus et al, 1997). Nonetheless, mixtures form mediums of bi-modal particle size distribution, the interplay of frame and bonding element within which controls the overall behaviour, that itself is fundamentally dependent on the relative proportion and properties of the constituting elements.

Buffers are designed for a hydraulic conductivity of $<10^{-9}m.s^{-1}$, a minimum admissible structural integrity (i.e. strength depending on the landfill geometry and adopted construction technique) and limited shrinkage cracking on moisture content variation which takes place during the service life of landfills (Tay et al., 2001). Studies of compressibility and strength in sand-bentonite composites were presented by Khoury et al. (1992) and Filz et al. (1999). The dependency of stress-state of consolidated sand-bentonite mixtures on compressibility and strength was surveyed in Evans et al., (1995). Blatz et al., (2002) and Romero et al., 2005 discussed the links between suction and microstructure. Tien et al. (2004) introduced one of the early forms of micromechanical models to be used in predicting the behaviour of compacted mixtures as a function of compaction conditions. The influence of compaction (i.e. placement) conditions on the potential of desiccation cracking were surveyed in the works of Kleppe and Olson (1985) and Tay et al. (2001). They suggested a critical threshold shrinkage strain of between 4% to 10% above which sand-bentonite buffers start to crack with serious unwelcomed implications. They collectively showed that desiccation shrinkage increases linearly with compaction water content and bentonite content and is unaffected by density. Saturation prior to desiccation increases strains markedly for specimens compacted dry of optimum. The effect of confining pressure on the swelling and hence hydraulic conductivity of composite buffers were studied in Graham et al. (1989) and Wiebe et al. (1998). In recent years, the coupled hydro-mechanical properties of clays have been studied by many workers. Delage and Cui (2008) showed that solid-fluid physiochemical interactions in clay control the soil water characteristic curve (SWCC) and hydraulic hysteresis. Vanapalli et al. (1999) showed that the SWCC has high reliance on the placement water content, in SWCC appearing in different forms for clays compacted using similar compaction effort but different optimum, wet of optimum, and dry of optimum water contents. Apart from a few attempts (Agus, 2005, Agus and Schanz, 2005a) and works on microstructure-based water retention properties in composite soils, little emphasis has been put into investigating hydromechanical properties in sand-bentonite mixtures. In hydro-mechanical modelling of composite soils, Ideally, the solid phase and the interaction between the two pore space phases (i.e. macro- and micro) need to be considered explicitly, so too the interaction between rigid solids (sand), elasto-plastic bonding (bentonite) and pore-fluids.

The concept of double porosity CDP (also known in earlier literature as dual-domain, dual-region or multi-region) has recently been adopted in explaining the coupled hydro-mechanical response of unsaturated buffer composites. In taking the CDP, heterogeneous microstructure of soil medium is assumed to consist of two and multiple independent but connected continua. The porous medium is divided into a number of domains that are coupled through an interaction term mainly for simulating the transport of fluids between pore systems or continuums (Barenblatt et al., 1960, Gwo et al., 1995). Based on the fundamental concepts of the *Concept of Double Porosity* (*CDP*), one proceeds from the hypothesis that pore spaces have two micro and macro constituents that whilst being inter-connected, deform independently as a function of matric suction. For structured bi-modal soil systems (not dissimilar to that of sand-bentonite), Assadi-Langroudi and Jefferson (2013) recently discussed the links between the hydraulic hysteresis and grading in composite granular soils. They suggested that the changes to soil's microstructure on cyclic wetting-drying is strictly limited to certain particle size intervals and is closely associated with certain pore size intervals. Thereby, certain pore size intervals control the matric suction. This highlights the significance of the *CDP*. As soil's water content changes, microstructure changes, so too the air values and shape of the SWCC. Wetting-drying cycles result in sequences of flocculation and dispersion. For a calcareous clayey silt (composing of 20% calcium carbonate, 10% Kaolinite and 70% negatively skewed quartz silt) oedometric specimen, Assadi-Langroudi and Jefferson (2013) showed that the change to soil's micro-structure on the first wetting-drying cycle is restricted to sub-20µm particle size interval, associated with the 0.02 to 3.55µm pore size interval, at which micro-fabric and thus soil water retention is most sensitive to slightest alterations in water content. On the dry stress-state surface, flocculation, dispersion, and grain breakage is most pronounced at 5 to 20µm particle size range. On wetting, changes to soil's micro-fabric is most pronounced at 20 to 30µm and sub-1µm particle size intervals. In addition to the shortfall in research into the hydraulic hysteresis in Sand-Bentonite systems, implications of shape and gradation of the sand constituent has also received very little attention. The particle and pore size distribution is an important micro-scale property that is associated with hydromechanical soil properties, including soil water retention and hydraulic permeability, skeletal compressibility and hydraulic hysteresis, all needed in design of liner systems. Predictive equations for soil water retention capacity based on the particle and pore size distribution have been presented in Arya and Paris, 1981, Juang and Holtz, 1986, Arya and Paris, 1982, Haverkamp and Parlange, 1982, Arya et al., 1999, Romero et al., 1999, Fredlund and Wilson, 1997, Mingbin et al., 2009.

To better understand the hydromechanical response and their anomalies in bi-modal sand-bentonite system, this contribution reports on findings from a comprehensive experimental programme. This paper surveys the hydromechanical properties of compacted sand-bentonite mixtures. It presents laboratory-scale experimental data on the hydraulic conductivity, water retention capacity, strength, large-strain stiffness, compressibility, compressive wave velocity, swelling and shrinkage (in two and three dimensions) of optimum compacted specimens and discusses the observations and anomalies. It is proposed that the complex, and often unexpected trends seen in the hydromechanical behaviour of sand-bentonite mixtures can be fully explained and hence predicted in the context of the Concept of Double Porosity. Sand particles' shape and mutual packing state controls the microfabric of sand-bentonite composite material, thereby controlling the hydromechanical characteristics of buffers.

2. Materials and Methods

The sands used were Crushed Limestone from Beşparmak Mountains, North Cyprus, having 50% particles finer than 1.14mm (well-graded), and Sea Sand from Golden Beach, North Cyprus having 50% particles finer than 0.29mm (poorly-graded). Figure 1a shows the particle size distribution of the sand constituents. The clay was supplied by Karakaya Bentonite Inc. Turkey, which is quarried at Uzunisa-Ordu as a sodium bentonite clay (conforming with the TS EN 13500 non-treated). The mineralogical composition of the clay used is demonstrated in the X-Ray Diffraction spectra of Fig 1b. Cu cathode tube was used, generating high-energy short-wavelength radiations (about 1.54 Å) were applied to decrease the attenuation in air and hence the absorption by the soil sample. The Bragg's Law ($n\lambda=2d\sin\theta$) and the reference of mineral powder diffraction data were used to identify the target mineral types. The d-spacings of interest included the 1.31 to 7.17 Å range for kaolinite, 1.83 to 3.58 Å for carbonates, and 1.38 to 4.26 Å for quartz ($n=1$, $\lambda=0.0061$ nm, $V=40$ kV). The X-Ray Fluorescence analysis was used to detect elemental and chemical composition of the Bentonite component of test specimens. XRF (X-Ray Fluorescence) technology involves in detection of the emitted secondary (i.e. fluorescent) X-ray from a material, after excitement by high-energy X-ray or gamma ray. Analysis suggested that the natural Bentonite comprised of 61.3% SiO_2, 17.8% Al_2O_3, 3% Fe_2O_3, 4.5% CaO, and 2.7% Na_2O.
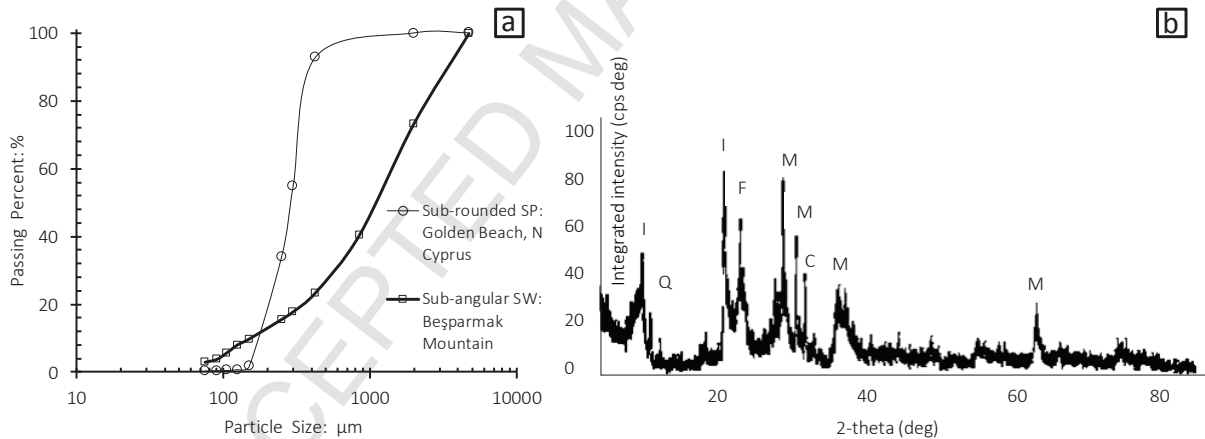

Figure 1 [a] Particle size distribution of sand fragment, [b] X-Ray Diffraction micrograph for Bentonite: [I=Illite; Q=Quartz; F=Feldspar; C=Calcite; M=Montmorillonite]

Sand-bentonite mixtures were prepared by adjusting the grading to contain pre-determined proportions in the sand and clay size ranges. Mixtures of air-dried clay with sand were prepared containing 0, 15, and 25% clay, based on the oven-dry weight, to form six compositions. Particle size distribution parameters and index properties were measured in compliance with the ASTM procedure and are outlined in Table 1. Dry sand-clay powder was thoroughly mixed with predetermined mass of deionized water for at least 7 minutes to permit the water to become uniformly distributed; wet mixes were then allowed to stand for at least 24 hours between initial mixing and specimen remoulding in sealed plastic bags. Wet mixes were

brought to the optimum water content and compacted using the standard proctor compactive effort to remould testing specimens (of varied dimensions).

Table 1. Composition and physical properties of test specimens and their constituents: USCS = Unified Soil Classification System

	Composition			G_s	D_{10}	D_{30}	D_{50}	D_{60}	C_u	C_c	USCS	LL	PL	PI	$\gamma_{d(max)}$	w_{opt}
	Sand		Clay	-	mm	mm	mm	mm	-	-	-	%	%	%	$kN.m^{-3}$	%
	S-R[1]	S-A[2]														
S1	100	0	0	2.88	0.18	0.24	0.29	0.32	1.78	1.00	SP	NPI	NPI	NPI		
S2	0	100	0	2.74	0.17	0.59	1.14	1.5	8.82	1.37	SW	NPI	NPI	NPI		
S3	85	0	15	2.70								74	22	52	16.6	17.0
S4	75	0	25	2.64								93	24	70	17.2	15.0
S5	0	85	15	2.79								64	21	44	18.5	14.0
S6	0	75	25	2.74								104	24	80	17.9	12.0
S7	0	0	100	2.51								461	41	420		

[1] sub-rounded
[2] sub-angular

The experimental program included index, standard proctor compaction, unconfined compression and ultrasonic pulse velocity (stiffness at large strains), saturated and unsaturated hydraulic conductivity, oedometer (free and constant volume swelling), 1D consolidation and shrinkage (at many scales). Geochemical and mineralogical composition of the clay component was studied using XRD and XRF analysis. Scanning Electron Microscopy was used to build a conceptual micromechanical model showing the packing state of test specimens. Vertical aligned cubic soil samples were cut and viewed under a Philips XL-30 LaB6 (General purpose 50x50 millimetre stage SEM). Test samples were air-dried under ambient laboratory conditions (23±2°C) over a course of three to four weeks. Dried cubic samples were then split by hand into two pieces. The obtained semi-circular samples were split again, trimmed to 5-7 mm sectors. Samples were then installed on aluminium stubs via hardener and resin. Loose particles were removed from the surface by turning the stub upside-down, several times. Samples were vacuumed to 0.15torrs and then vacuum-coated with Platinum before imaging.

To further refine the micromechanical models, Soil water characteristic curves were built for the four main testing specimens. Filter paper test was adopted as the experimental technique to build the Soil Water Retention Curves for four main testing specimens (S3, S4, S5, and S6). The data from the filter paper test was then statistically processed using van Genuchten (vGM) and Fredlund and Xing (FX) models.

Filter paper test enables measurement of suction values in surplus of 1500kPa and is arguably the most widely used technique for measurement of suction for compacted soil samples. The sand-bentonite mixtures were compacted to maximum dry unit weight (using standard compaction effort) and saturated thereafter under 7kPa seating pressure in standard 50mm diameter oedometer rings. On completion of full saturation, the specimens were dried at room temperature (well-ventilated environmental room). Water content was frequently recorded along the drying course. The specimens were kept in intimate contact with Whatman No. 42 filter paper discs inside tightly sealed containers that were encapsulated in airtight Styrofoam boxes. The Styrofoam boxes were filled with glass wool and capped using sealing tapes to guarantee good insulation. The boxes were kept under constant 22°C temperature in an environmental chamber. Filter papers were weighed up every 7 to 10 days (equilibrium time) for suction determination. The matric suction – water content data was then fed into the van Genuchten (vGM) and Fredlund and

Xing (FX) models to build the SWRC curves. The Van Genuchten (1980) equation has been widely used by many workers, and is endorsed in Leong and Rahardjo (1997) and Fredlund and Xing (1994) as sets of equations that provide the finest SWRC models for a wide variety of soils. The equations are not equivalent to linear equations; the SWRC parameters were determined through nonlinear regression using a least-squares algorithm. The Soil Vision computer programme (Soil Vision Systems Ltd. 1999) was adopted for the regression analysis.

Equation 1 formulates the Fredlund and Xing (1994) model,

$$w(\psi) = c(\psi)\frac{w_s}{\left\{\ln\left[e + \left(\frac{\psi}{a}\right)^n\right]\right\}^m} \tag{1}$$

Where w(ψ) is the gravimetric unsaturated water content, w_s represents the saturated gravimetric water content, 'a' is a soil parameter linked to the Air Entry Value (AEV) (ψ_a), 'n' is a soil parameter relevant to the slope at the curvature point (near the air- entry value) on the SWRC, 'm' is a soil parameter related to the residual water content (also see Vanpalli, 1999), ψ is soil suction in kPa, and $c(\psi)$ is correction factor as given in Equation 2.

$$c(\psi) = 1 - \frac{ln\left(1 + \frac{\psi}{\psi_r}\right)}{ln\left[1 + \left(\frac{1000000}{\psi_r}\right)\right]} \tag{2}$$

Where ψ_r demarcates soil suction in kPa that corresponds with the residual water content (w_r). The *Air Entry Value* is the matric suction at which air commences to enter the largest pores in a soil (Fredlund and Xing, 1994) and occurs roughly at the SWRC's point of maximum curvature, which itself is dependent on the amount of water in soil (Fredlund et al., 2011) and hence the soil packing state.

The van Genuchten (1980) model is formulated in Equation 3:

$$w(\psi) = \frac{w_s}{\{1 + (a\psi)^n\}^m} \tag{3}$$

where w_s and ψ have the same definitions as in Equation 1, 'a' is a soil parameter linked to the *Air Entry Value* (*AEV*) (ψ_a), and 'n' is a soil parameter relevant to the rate of water removal from the soil, when the *AEV* has been reached. The SWRC curves were built to further refine the micromechanical models as fully discussed in Section 3.

3. Results

3.1 Packing State

It is believed that in specimens S3 and S4 (composite soil with well-graded sub-rounded sand fragments), illuviated clay platelets fully coat the smooth and rounded surface of sand particles. Coatings then extend and overlap to form inter-particle bridge units. Figure 2a shows the scanning electron microscopy image of specimen S3 at an intermediate magnification. A matrix of coated sub-rounded particles appears to have formed chains of quartz particles encapsulating large macro-pore spaces. In specimens S5 and S6 (composite soils with poorly-graded sub-angular sand fragments), clay platelets accumulate at particle

contact points due to the relatively higher matric suction that is stemmed from interlocking sharp asperities. Figure 2b illustrates the scanning electron microscopy image of specimen S5, where sub-angular quartz particles are clean and interconnected either via interlocking or clay aggregates at pore space trapdoors.
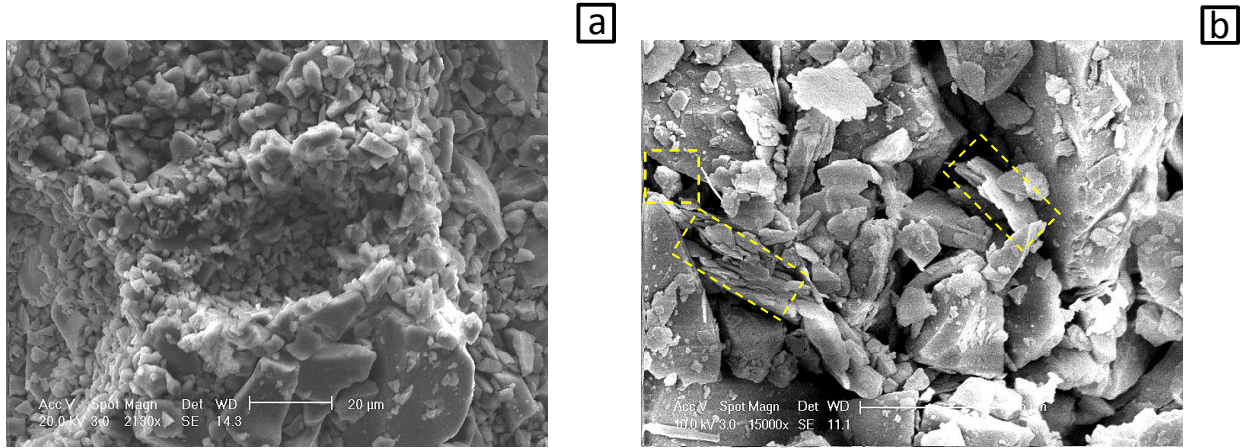

Figure 2 [a] SEM image showing chains of interconnected clay coated sub-rounded quartz grains, [b] SEM image showing lightly clay coated sub-angular quartz grains bridged by clay coagulates

This micromechanical model of the composite soils is graphically illustrated in Fig 3.
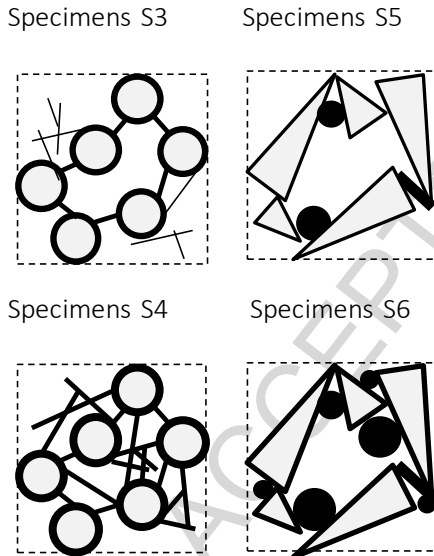

Figure 3 micromechanical model of specimen groups S3-S4 and S5-S6

3.2 Physio-mechanical Properties

It is intuitively agreed that physio-mechanical properties of composite geomaterials are a function of their quartz fragment's mean size, shape, grading (Assadi-Langroudi et al., 2014), and the packing state (i.e. microfabric). In accordance with the tenets of soil diagenesis, at low 15% clay content, rounded grains receive an even all-around clay coating whereas angular grains attract colloidal clay platelets at their sharp asperities, where clay then precipitates to form inter-particle coagulates, leaving behind a suite of

interlocking clean (uncoated) and thus permeable grain-grain contacts (Fig 3, Specimens S3 and S5). This explains the direct relationship between sands' roundness and liquid limit at low clay contents. At high clay contents, liquid limit attains an inverse relationship with roundness. Upon wetting, the clay coating units around spherical grains act as lubricants and facilitate the change in packing state to a denser fabric. Where clay fragments coat the sub-angular sand particles, the interlocking between quartz grains delay the wetting-induced packing state change, and hence the transition of soil from the semi-solid state into liquid (Fig 3, Specimens S4 and S6 – also see figures 2a and 2b).

Higher orders of maximum dry density were achieved in specimens with sub-angular well-graded sand fragments. This shows the significance of particle shape in the packing state upon compaction. Higher orders of optimum water content were achieved at lower clay contents, which can be invoked to account for the absence of clay agglomerates at macro-pore phase, regardless of particle shape. This re-emphasis on role of changing clay content on rebalancing macro- and micro-pores relative proportion. The role of particle size and shape on large strain stiffness is demonstrated by unconfined compressive strength and ultrasonic pulse velocity test results combined. The results indicate that the unconfined compressive strength, elasticity modulus (large-strain stiffness) and compressive wave velocity are directly correlated with clay content. This can partly be due to the formation of long-range bonds. The implications of long-range bonds are more pronounced when the sand fragment is of larger size, well-grading, and high angularity (Table 2).

The influence of particle-level characteristics on compression was studied through 1D-oedometer tests on the four main composite mixtures (compacted at optimum water content). Specimens were initially allowed to swell under 7kPa seating pressure. The swelled specimens were subsequently loaded, incrementally and under confined condition, following the standard ASTM consolidation protocol. Consolidation parameters drawn are reported in Table 2. The implications of bi-modal composition of testing specimens are reflected in the tri-linear form of the $e - log\sigma'$ curves (Fig 4a). Observations are consistent with the trends reported in the earlier work of Stewart et al. (2003). Particle shape appears to have no effect on the slope of the virgin (normal consolidation) line (m_1 and m_2 – compression index) and only a marginal effect on the slope of the rebound line (m_3 – swelling index) at low clay contents (Fig 2d). This is possibly due to the predominant frictional behaviour of soil at low clay contents and ties in with our earlier observations in the relationship between consistency limits, particle shape and clay content. The pronounced influence of sand particles interlocking for 'small clay' angular sand specimens also led to relatively lower order of consolidation settlement (in comparison with identical samples comprising sub-rounded sand particles).

Table 2. Strength, stiffness, and compressibility parameters: ε_f=strain at failure, E=Young's Modulus, C_u= Undrained cohesion, q_u= Unconfined compression strength, V_p = compressive wave velocity, C_c= Compression index, C_s = swelling index

Specimen	ε_f %	E $kN.m^{-2}$	V_p $m.s^{-1}$	C_u $kN.m^{-2}$	q_u $kN.m^{-2}$	C_c m_1	m_2	C_s m_3
S3	11.3	2070.8	586	117.0	234.0	0.5	0.2	0.02
S4	8.1	4228.4	913	171.5	342.5	0.6	0.4	0.02
S5	13.3	1872.2	664	124.5	249.0	0.5	0.2	0.01
S6	9.0	5355.5	1144	226.5	482.0	0.8	0.8	0.04

Free swelling index (from confined free-swelling test) is plotted against the logarithm of wetting time in Fig 2c (also see also Table 3). Swelling index almost doubled for a 10% increase in clay content (from 15 to 25%). The higher swelling potential is attributed to the activity of the Bentonite clay mineral. The time required for primary swelling to fully take place was also found directly proportional with the Bentonite content. Higher rates of the secondary swelling were logged at enhanced clay contents. Figure 2c suggests that angularity of sand fragment can improve the swelling potential, swelling pressure, and swelling rate. This could be partly due to the dilation effect. In structured soils with poorly sorted angular sand component, there are large inter-assemblage pores that are bonded with clay bridges. When clay component swells, there is little chance for the macro-pores to fully contract. This can further enhance the swelling potential. Greater swelling potential is welcomed when sand-bentonite mixtures are used as a component of clay liners. Greater placement dry unit weight and lower water content for specimens with crushed limestone sand could be a reason for the captured greater swelling. This is generally consistent with previous findings (see El-Sohby and Rabba (1981), Assadi-Langroudi and Yasrobi (2009)).
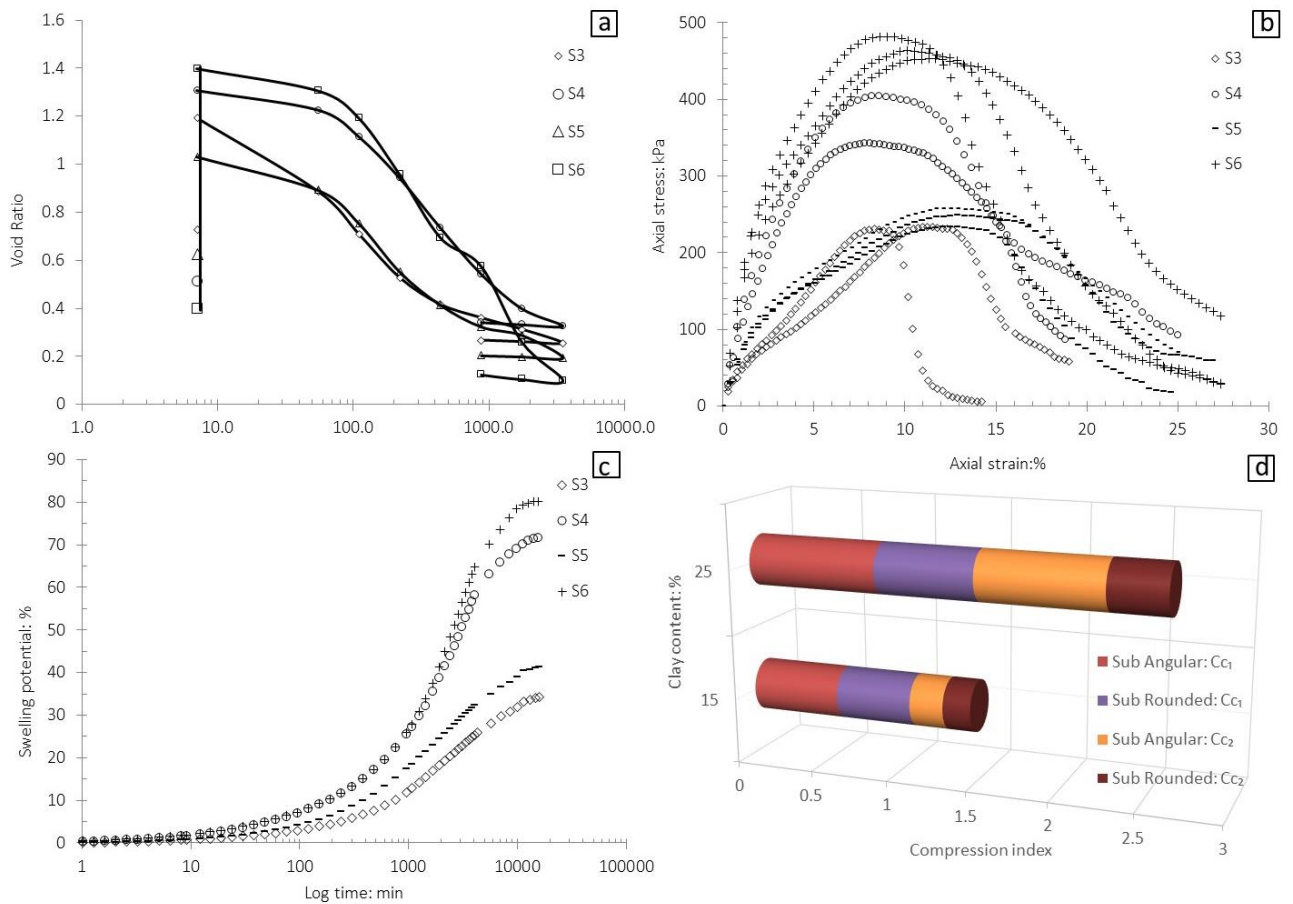

Figure 4. [a] 1D consolidation e-logσ' curve, [b] stress-strain patterns from unconfined compressive strength experiments, [c] swelling potential curves, [d] Variation of compression and swelling index

Saturated hydraulic conductivity of sand-bentonite mixtures was measured indirectly using the standard 1D consolidation equations. Measured permeability values were generally low, possibly because of the clay fragment of soils coating and encrusting the quartz grains and pore network (also see Kumar and Yong (2002)). Clay content is inversely proportional with the saturated permeability, highlighting the role of clay fragment in limiting the flow through soil's pore network. Greater angularity in sand was found to decrease the saturated permeability, exhibiting the role of sharp sands in interlocking and blocking the water pathways.

Table 3. hydro-mechanical properties: i_s= Primary swelling index, t_s= Elapsed time for completion of primary swelling, σ_p= Constant volume swelling pressure

Specimen	i_s %	t_s %	σ_p kPa	K_{sat} m/s	
				7-880kPa	880-3520kPa [*]
S3	28	5000	80	9.81E-09	4.13E-10
S4	64	6000	850	1.45E-09	1.35E-10
S5	40	7900	131	2.85E-09	1.71E-10
S6	82	10000	1092	6.09E-10	1.16E-10

[*]Load steps of the oedometric test

3.2 Structure-based Soil Water Retention and System Serviceability

Compacted sand-bentonite composites are commonly used as liners in waste-containment structures as barriers in between groundwater and buried contaminants. The in-service water content in liners frequently vary, so too their volume. Loss of water often results in shrinkage and formation of unwelcomed cracks, the characteristics of which can be determined from Soil Water Retention Curves (SWRC) and shrinkage curve (i.e. gravitational water content versus void ratio) combined. A knowledge of soil's hydraulic properties is needed for better flow and contaminant transport modelling.

3.2.1 Soil-water Retention Curve

This section introduces experimental and numerical methods used to capture hydraulic properties of testing composite materials, and discusses the results from a micro-to-macro perspective. The Soil Water Retention Curve relates the soil matric suction ψ to water content (by mass or volume). In desorption phase, water content of a soil decreases with increasing soil suction (i.e. drying protocol).

Filter paper test was adopted as the experimental technique to build the SWRC curves for the four testing specimens. The data from the filter paper test was then statistically processed using van Genuchten (vGM) and Fredlund and Xing (FX) models.

The SWRCs are drawn using fitting parameters from Equation 2 and Equation 3, through best-fitting of the filter paper test data using a least-squares algorithm (Van Genuchten 1980; Fredlund and Xing, 1994). Filter paper tests were conducted in compliance with the drying protocol (Fig 5a-b). The residual water content, *AEV*, and fitting parameters of the SWRCs and summarized in Table 4. The *AEVs* in specimens with sub-rounded well-sorted sand were found to be greater than *AEVs* in specimens of similar clay content but sub-angular poorly-sorted sand.
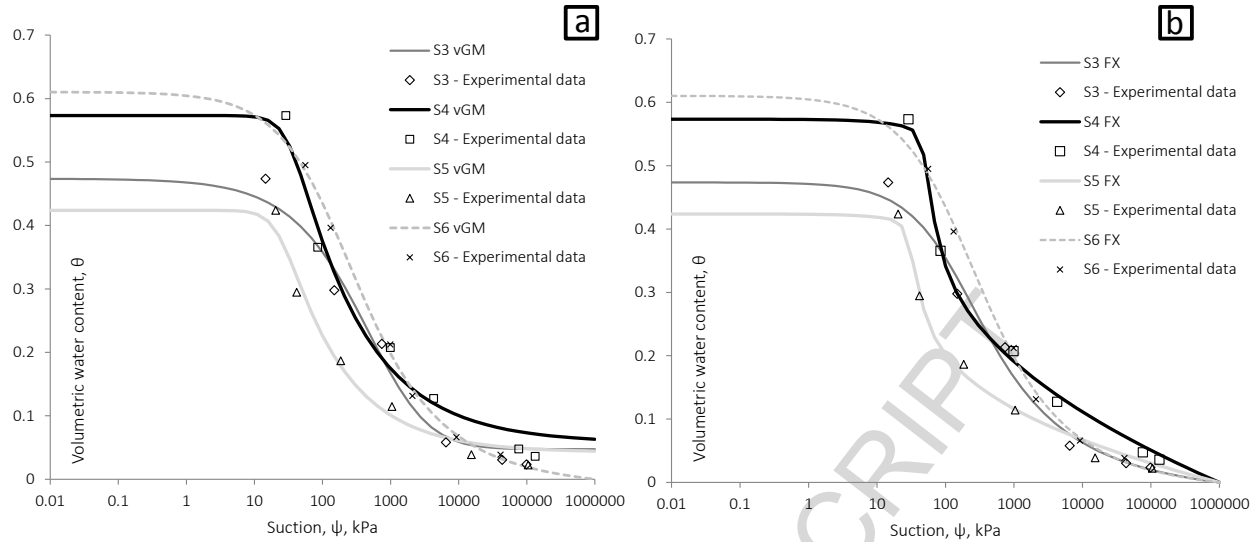
Figure 5: Soil Water Retention Curves [a] fit to van Genuchten (vGM) model; [b] fit to Fredlund and Xing (FX) model

Table 4. Water Retention properties for the four testing specimens via van Genuchten (vGM) and Fredlund and Xing (FX) models: 'a', 'n' and 'm' = soil parameters, w_r = residual water content, h_r = residual suction in kPa, R^2 = Coefficient of Determination, AEV = Air Entry Value.

Specimen	Fredlund and Xing (1994)							Van Genuchten (1980)					
	a	n	m	h_r	R^2	w_r: %	AEV: kPa	a	n	m	R^2	w_r: %	AEV: kPa
S1							1.632[1]						
S2							0.533						
S3	120.8	0.93	1.18	2320.32	0.985	8.0	27.10	0.0005	0.6939	2.486	0.977	10.0	33.28
S4	48.29	7.81	0.26	130.70	0.996	23.9	39.37	0.0300	3.0000	0.145	0.975	10.0	24.30
S5	28.91	6.95	0.30	84.48	0.992	16.0	23.22	0.0429	3.0000	0.166	0.976	10.0	17.14
S6	133.3	0.82	1.46	2505.34	0.996	8.2	21.22	0.0002	0.6052	4.877	0.993	10.0	24.30

[1]Fredlund and Wilson 1997 Pedo-Transfer Function model

In Fig 6, average values of volumetric, axial, and diametric strains are plotted against drying time. The samples were compacted at optimum water content to maximum dry unit weights, and left to swell completely. The majority of shrinkage in soils was recorded within the first 6 days (8000 min). The results infer that clay inclusion decreases the shrinkage rate and increases elapsed drying towards maximum strains by 25%. Generally, the shrinkage rates decreased with drying time to almost zero by the eighth day (11000min). Shrinkage strains were found to be directly correlated with clay content and angularity of sand fraction (Fig 6d). Axial shrinkage strains were found to be double the value of diametric strains (Fig 6b, 6c).
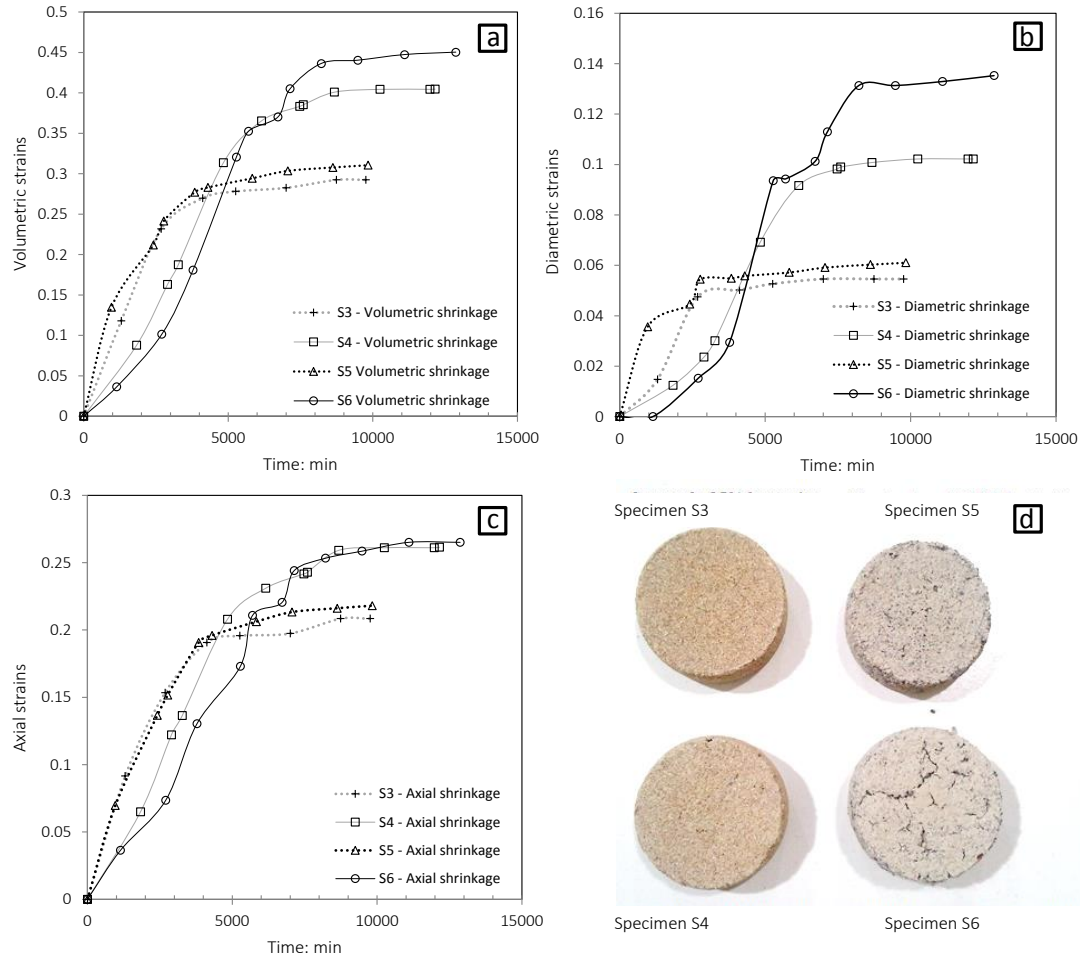
Figure 6: Shrinkage and crack formation. [a] timed growth of volumetric strains, [b] timed growth of diametric strains, [c] timed growth of axial strains, [d] End-of-test crack patterns

3.2.2 Shrinkage Curve

Excessive tensile strains can trigger cracking in soils. Tensile strains can be stemmed from soil shrinkage on desiccation following loss of bulk water. In effect, cracks form when horizontal tensile strains caused by coagulation of clay platelets exceed beyond a threshold tensile strain, which is predominantly controlled by soils geochemical composition. Shrinkage limit in definition is the water content at soil's minimum attainable volume (equivalent to the residual water content), and is generally expected to fall slightly below the plastic limit (Fredlund et al., 2011). The Shrinkage curve is obtained experimentally by reducing the water content from an initially high to an entirely dry condition. The shrinkage curves have a significant role in the explanation of SWRC results.

Sand-bentonite mixtures compacted at their optimum water contents and saturated in oedometer cell (following one-dimensional swelling-consolidation) were air-dried and allowed to shrink at room temperature (22-25°C). The specimens were weighed periodically, and the average diameters and heights were recorded using a high precision Vernier calliper until specimens dried to their residual water contents. The water content and volumetric shrinkage were captured and calculated during and after

drying to generate the shrinkage curves (Fig 7). Through the drying/desiccation path, volume of water gradually decreased, thereby $e - w$ curves cut through the degree of saturation contour lines from 100% to 60%.
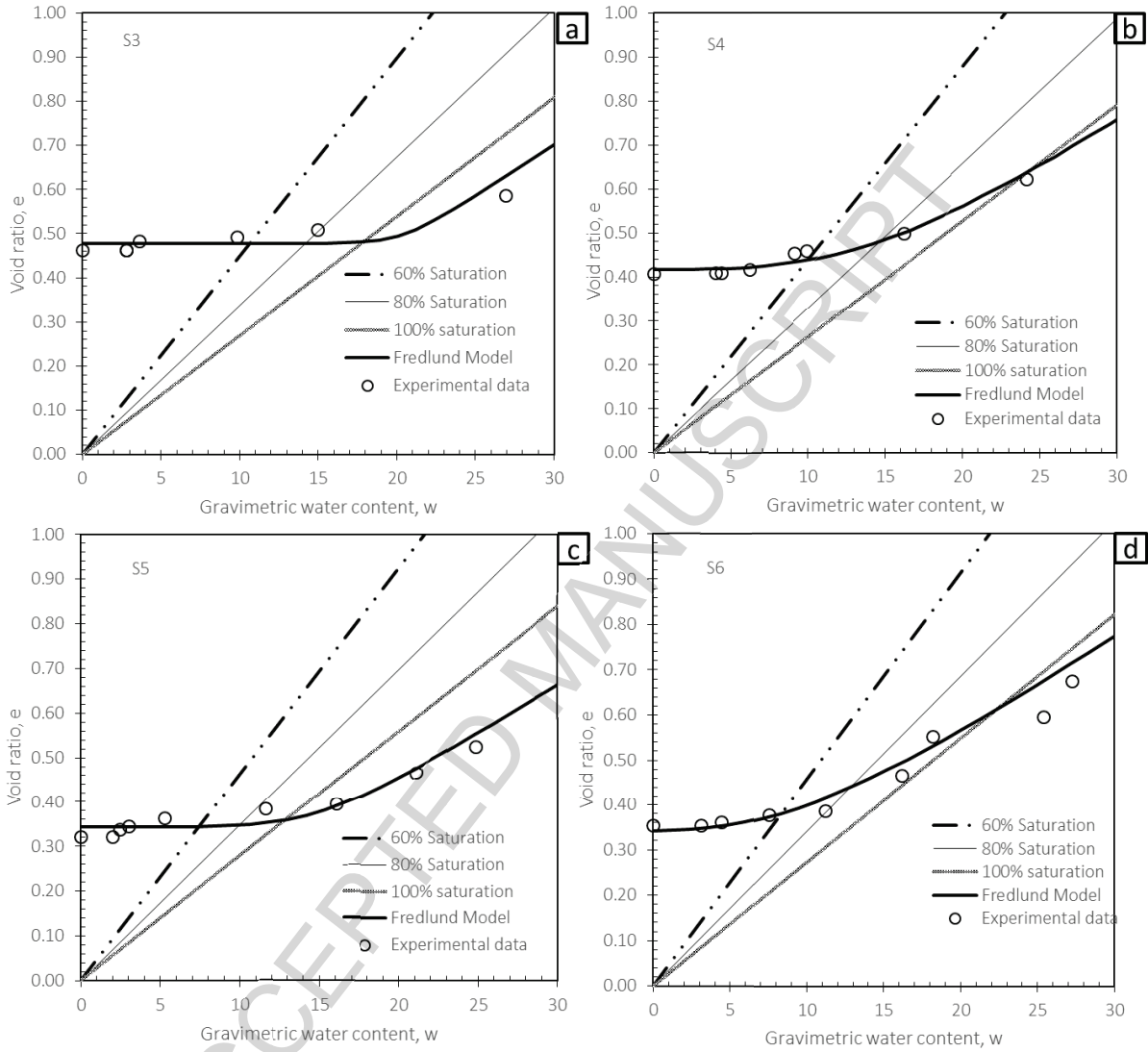

Figure 7 Shrinkage curves of composite sand-bentonite mixtures

The Soil Vision computer software (Soil Vision Systems Ltd. 1999) was used to plot the hyperbolic-shaped shrinkage curves. The software made use of the Frenlund et al. (1997, 2002) model for fitting the data from experiments (Equation 4).

$$e(w) = a_{sh} \left[\frac{w^{c_{sh}}}{b_{sh}^{c_{sh}}} + 1 \right]^{\frac{1}{c_{sh}}} \tag{4}$$

Where, a_{sh} is the minimum void ratio (e_{min}), b_{sh} is slope of the tangent line (to $e - w$ curve), c_{sh} is the curvature of the curve, and w is the gravimetric water content. Here, the relationship between void ratio

and water content (i.e. shrinkage curve) was determined from captured volume change data, and is presented in Fig 7 alongside the degree of saturation contour lines (60%, 80% and 100%).

The shrinkage curve supplies volumetric insights for a soil as it desiccates, whereby volumetric properties of soil can be calculated. Once fitted with the hyperbolic equation, the shrinkage curve allows an assessment of soil water-content-related volumetric properties. The fitting parameters for the four testing specimens are specified in Table 5. Clay content and angularity of sand fraction appeared to be inversely proportional to the shrinkage limit (S_L) and minimum void ratio (e_{min}). The difference between shrinkage limit and plastic limit increases with increasing clay content (Fig 7) and changes sands shape/grading.

Table 5: Fitting shrinkage parameters calculated using Soil Vision: a_{sh} = minimum void ratio, b_{sh} = slope of the tangent line to $e - w$ curve, c_{sh} = curvature of the $e - w$ curve, R^2 = Coefficient of determination, S_L shrinkage limit

Specimen	a_{sh}	b_{sh}	c_{sh}	R^2	S_L: %
S3	0.478	0.204	16.669	0.9887	0.20
S4	0.417	0.174	3.181	0.9956	0.17
S5	0.344	6.029	6.029	0.9901	0.16
S6	0.342	2.306	2.306	0.9886	0.14

3.2.3 Hydraulic Conductivity

One other key design input parameter in clay liner systems is the unsaturated hydraulic conductivity which varies with soil suction (Fredlund et al. 1994). Van Genuchten established a closed-form equation (vGM) for the relative hydraulic conductivity function ($k_r=k_\psi/k_s$). Mualem (1986) revised the Van Genuchten equation into the statistical relative hydraulic conductivity model (MLM) that is described in Equation 5.

$$k_r = \frac{\{1 - (\alpha\psi)^{n-1}[1 + (\alpha\psi)^n]^{-m}\}^2}{[1 + (\alpha\psi)^n]^{\frac{m}{2}}}$$ (5)

Where ψ represents any soil suction value in kPa, and α, n, and m are constant values.

The estimated unsaturated hydraulic conductivity is plotted against soil suction using the vGM and MLM models in Fig 8. At low suction values, the mixtures with sea and crushed limestone sand with 15% bentonite content gave the highest permeability (in comparison with mixtures with 25% bentonite). The low hydraulic conductivity seen in mixtures at high pressures is probably due to compression of sand and bentonite particles and the subsequent decrease in void ratio. A zero unsaturated hydraulic conductivity was recorded for all sand bentonite samples at high suction. Clay content and sand fraction angularity appeared to be inversely proportional to the unsaturated hydraulic permeability.
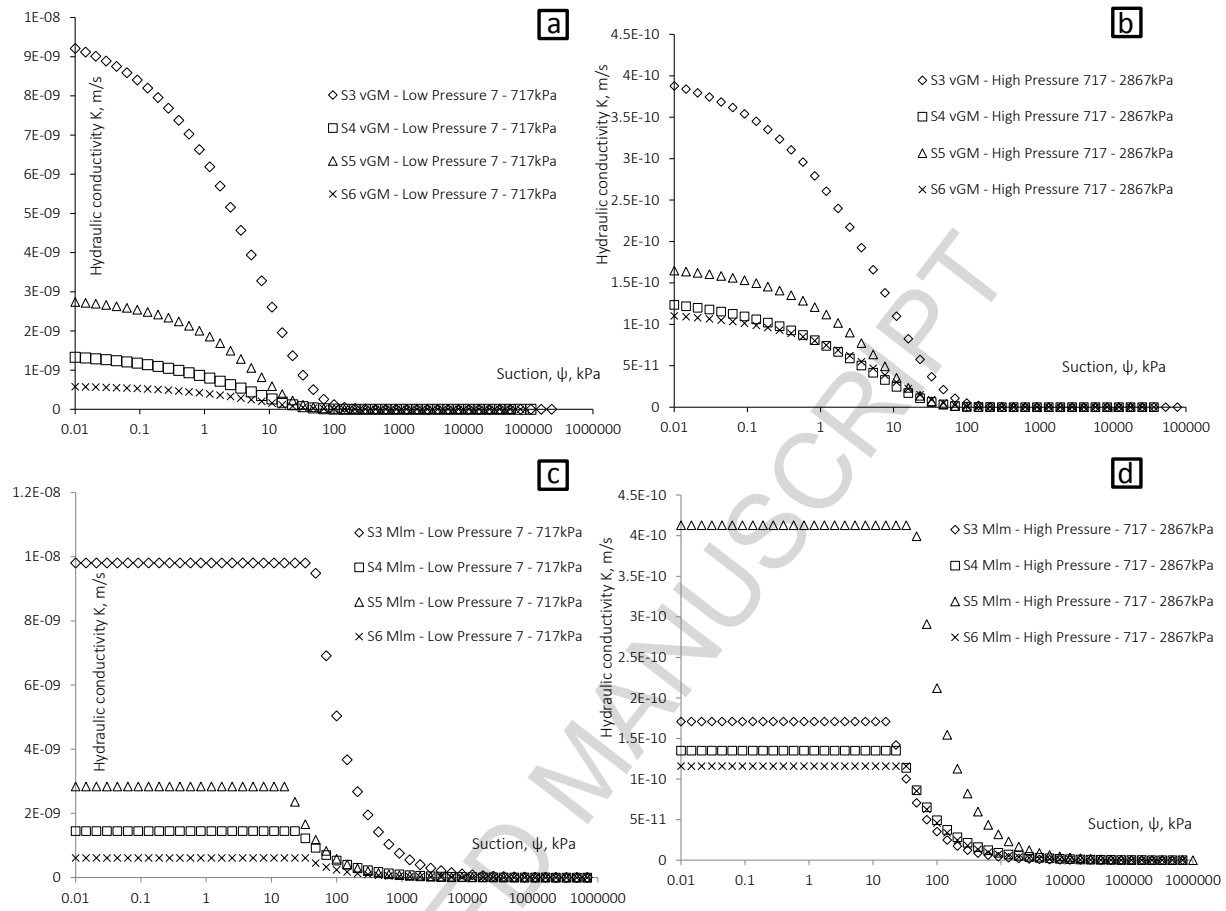
Figure 8 Suction controlled hydraulic conductivity

4. Discussion

Properties of composite geomaterials are controlled by their quartz fragment's mean size, shape, grading and the packing state (i.e. microfabric). From a micromechanical perspective, assuming a constant void ratio, a variation in clay content in sand-bentonite system will rebalance the macro- to micro-pores volume ratio. The subsequent alteration in the packing state however is controlled by sand particles shape and sorting. This section will chiefly examine the evidence as to whether the 'Small Clay – Large Clay' conceptual model proposed in Jefferson and Smalley (1995) - and had been crystallized before by many, unconsciously perhaps - might explain the physio-mechanical and hydro-mechanical properties of sand-bentonite systems too.

4.1 Physio-Mechanical Characteristics

At low clay contents (i.e. 'Small Clay'), sand particles shape/grading were found not to have any control on the compression index, and only a marginal control on the swelling index of soils. This was attributed to the implications of particles' interlocking and dominant frictional behaviour of soil in at low clay

contents. The interlocking is supplied by clean sand particles in direct contact, as clay fragments in 'Small Clay' system tends to be mainly accommodated at macro-pore phase. This layout also led to higher orders of optimum water content for 'Small Clay' specimens regardless of particle shape, as bulk water extends from micropores into macro-pores within inter-assemblage spaces.

The threshold between frictional and non-fictional soil behaviour has received considerable attention. Jefferson and Smalley (1995) used an R-diagram framework to show soil behaviour is predominantly frictional when the 'bond to weight ratio R' drops to orders less than 1. They also claimed that for soils with an R≥1, the behaviour remains predominantly frictional and that increasing clay content initially produces short-range bonds (i.e. 'small clay' category). More recently, Assadi-Langroudi (2014) showed for loessic soils that soils with clay contents lower than 30% fall in the 'small clay' category. They surveyed the effect of particle shape on compressibility of clayey silts (with sub-angular silt grains), using transient loading-unloading oedometric experiments. For 'small clay' soils, they showed that the slope of the rebound line (swelling index) only marginally changes on varying clay content (6.3% and 6.2% rebound for 5% and 20% clay content). From a *Double Porosity Concept* perspective, an excess negative pore water pressure forms upon unloading and subsequent decrease in net stress (also see Fredlund and Rahardjo, 1993). This generates a pressure gradient, allowing pore water to flow from the macro-pore spaces into the micro-pore spaces. Clay intra-lattice spaces expand, pushing neighbouring quartz grains to move apart and triggering an elastic rebound. For testing specimens used in this study fit the 'small clay' class, clay platelets can be found in form of coagulate units at the sharp contact points of clean sand grains (Fig 2b, 3). Upon unloading the elastic rebound takes place predominantly due to dilation. Clay coagulates expand on absorbing the macro-pore water into macro-pore spaces (Fig 2b).

On transition of composite soils to 'Large Clay' from 'Small Clay', large strain stiffness and strength increase, due to the formation of long-range bonds. The latter bonds are stronger in presence of coarser angular sand fragments of well-grading. Whilst grain asperities enhance the strength of the composite materials, higher angularity also leads to greater degrees of swelling potential/pressure, volumetric, axial, and diametric shrinkage strains on moving from 'Small Clay' to 'Large Clay'. These observations were in agreement with relatively greater void ratios measured for specimens with sub-angular sand particles ('Large Clay') on the drying path.

4.2 Hydro-Mechanical Characteristics

The *AEVs* in specimens with sub-rounded well-sorted sand were found to be greater than *AEVs* in specimens of similar clay content but sub-angular poorly-sorted sand. For a constant total volumetric water content, composite soils with sub-rounded well-sorted sand fragment tend to have lower micro-level volumetric water content (θ_m) than that in identical composite soils with sub-angular poorly-sorted sand fraction. Air enters the macro-pores as θ_m tends to the residual. The air entry values derived from the Fredlund and Xing (1994) model are directly related to clay content in specimens containing sub-rounded well-sorted sand. This is consistent with the direct relationship established between liquid limit and clay content in presence of sub-rounded sand particles, and infers a close link between clay coating quality, particle shape, and the water retaining capacity. The relatively greater number of desiccation cracks in sand-bentonite composites with fine sub-angular sand (see Fig 6d) agrees with the decrease in the *AEV* from 23.2% to 21.2% on increasing bentonite content. The van Genuchten (1980) model could

not establish the links between particle shape and *AEV*, thereby was less compatible with composite bi-modal soil systems, where particle shape plays a key role.

Figure 9 illustrates the variation of void ratio with suction for testing specimens on the drying path. On examining Figure 9 in conjunction with Figure 7, the matric suction at shrinkage limit was approximated to fall within 1300 to 2100kPa range for specimens with sub-rounded sand fragments, and 110 to 3500kPa range for specimens with sub-angular sand fragments. The suction at shrinkage limit is directly correlated with clay content.
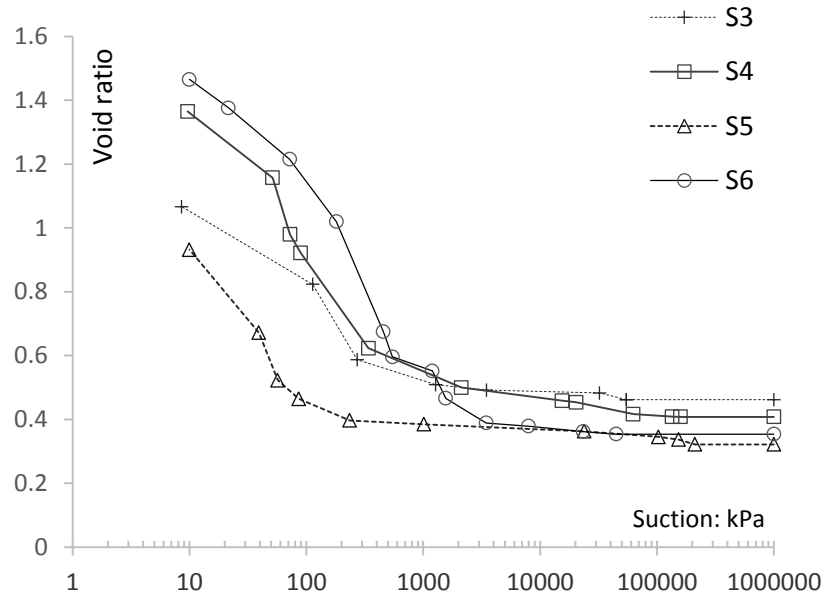

Figure 9 Variation in void ratio with suction on the drying path

5. Conclusion

Although previous studies have suggested for Sand-Bentonite buffer systems that sand's size and shape almost always control the hydromechanical properties of geo-composite materials, this study demonstrates clear evidence for a threshold clay content below which size, shape, and sorting of frame elements (i.e. sand) have a marginal control; This threshold clay content is here demonstrated to induce two types of discretely different packing state.

Core to understanding the behaviour of bi-modal composite geomaterials is a knowledge of structure-based and suction-related physical, mechanical and hydraulic properties. An experimental programme was designed and performed to survey links between hydromechanical properties and microstructure for compacted sand-bentonite mixtures. Experimental results were presented for four main soil compositions commonly used in clay liner systems: compacted specimens of sand-bentonite made up of two different sand types (in shape, size and sorting) and bentonite content in range of 15 to 25%. A comparison shows that there is a fair measure of agreement between the findings here and similar previous published attempts. Sivapullaiah and Sridharan (1985) argued that there is more to sand particle

shape than sand particle size. It merits some discussion because it is possible that whilst grain size is indeed critical in determining the behaviour of sand-bentonite composite mixtures, over-emphasis on particle size and taking a purely macro-mechanical approach, deflects attention from the central fact that shape, size, sorting and fine-fraction combined control the hydro-mechanical response of composite geomaterials.

Comprehensive experimental analysis of four sand-bentonite mixtures have differentiated two types of composite geomaterials, 'Small Clay' and 'Large Clay'. 'Small Clay' composite soils are frictional as macropores house the clay coagulates, thereby, sand size, shape, and sorting gains only marginal importance in the order of optimum compaction water content, compression, rebound, shrinkage, and swelling properties, as these are dominantly controlled by the clay fraction of soils. Sand-Bentonite mixtures are however bi-modal (in particle and pore size distribution), thereby exhibiting structure-based hydromechanical properties when unsaturated. These enhance the control of sand size, shape and sorting on air entry value, hydraulic hysteresis, hydraulic conductivity, and suction at shrinkage limit. As such, the pattern, likelihood, and order of desiccation cracks in compacted sand-bentonite fills can be moderated by informed design of sand fraction, that includes sand size, shape and sorting as well as mass content. At high clay content and 'large clay' composites, sand with angular shape has higher compression and swelling index, constant volume swelling pressure and swelling rate, unconfined compression strength and large strain stiffness. Angularity decreases the shrinkage limit, saturated and unsaturated hydraulic conductivity, and lowers the air entry value. Presence of angular sand fragment adds to the likelihood and extent of desiccation cracking, increases the shrinkage strains (axial, diametric and volumetric), and decreases the shrinkage limit and minimum void ratio. The effect of sand's particle shape on soil's consistency limit is dependent on the clay content. A summary of findings from this study is schematically presented in Fig. 10.
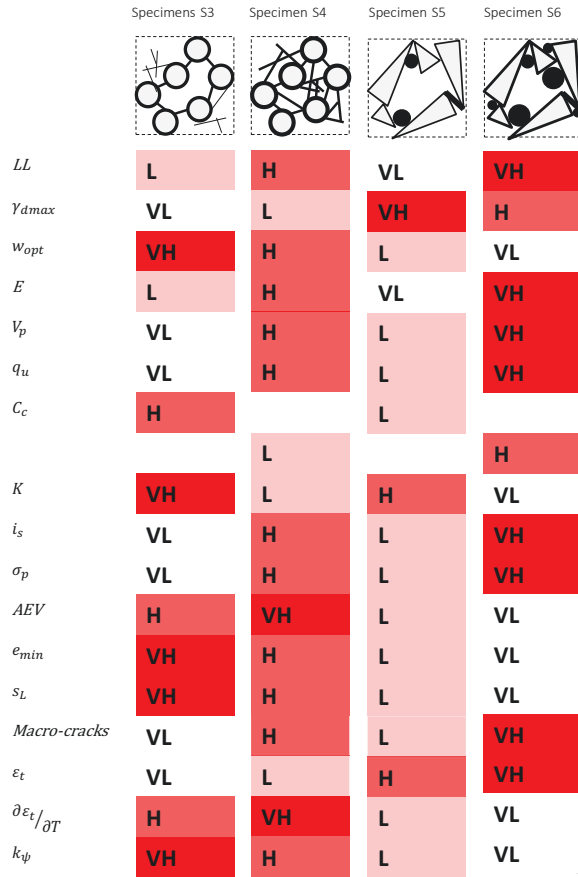
Figure 10 Dependency of hydromechanical properties on particle shape

	Specimens S3	Specimen S4	Specimen S5	Specimen S6
LL	L	H	VL	VH
γ_{dmax}	VL	L	VH	H
w_{opt}	VH	H	L	VL
E	L	H	VL	VH
V_p	VL	H	L	VH
q_u	VL	H	L	VH
C_c	H		L	
		L		H
K	VH	L	H	VL
i_s	VL	H	L	VH
σ_p	VL	H	L	VH
AEV	H	VH	L	VL
e_{min}	VH	H	L	VL
s_L	VH	H	L	VL
$Macro\text{-}cracks$	VL	H	L	VH
ε_t	VL	L	H	VH
$\partial\varepsilon_t/\partial T$	H	VH	L	VL
k_ψ	VH	H	L	VL

References

Arya, L.M., Leij, F.J., Van Genuchten, M.T. and Shouse, P. J. 1999. Scaling parameter to predict the soil water characteristic from particle-size distribution data. Soil Science Society of America Journal, 63, 210-519.

Arya, L.M. and Paris, J.F. 1982. Reply to comments on: A physicoempirical model to predict the soil moisture characteristic from particle-size distribution and bulk density data. Soil Science Society of America Journal, 46, 1348-1349.

Arya, L.M. and Paris, J.F. 1981. A physicoempirical model to predict the soil moisture characteristic from particle-size distribution and bulk density data. Soil Science of America Journal, 45, 1023-1030.

Assadi-Langroudi, A., Jefferson, I, O'Hara-Dhand, K., and Smalley, I. 2014. Micromechanics of quartz sand breakage in a fractal context. Geomorphology. 211, 1-10.

Assadi-Langroudi, A. and Jefferson, I. 2013. Packing quality and water retention properties on stress state surfaces in calcareous clayey loess. International Journal of Geomaterials, 5(1), 619-626.

Assadi-Langroudi, A., and Yasrobi, S.S. 2009. A micro-mechanical approach to swelling behavior of unsaturated expansive clays under controlled drainage conditions. Applied Clay Science. 45 (1-2), 8-19.

ASTM D2435. 1965. Standard Test Methods for One-Dimensional Consolidation Properties of Soils Using Incremental Loading. Annual Book of ASTM Standards, 04.08, Soil and Rock; Building Stones - 4, ASTM, Philadelphia, PA.

ASTM 1997. Annual Book of Standards, Soil and rock, ASTM International. West Conshohocken. PA.

ASTM D2166-06. 1963. Standard Test Method for Unconfined Compressive Strength of Cohesive Soil. Annual Book of ASTM Standards, 04.08, Soil and Rock; Building Stones - 4, ASTM, Philadelphia, PA.

ASTM D4318-10. 1983. Standard Test Methods for Liquid Limit, Plastic Limit, and Plasticity Index of Soils. Annual Book of ASTM Standards, 04.08, Soil and Rock; Building Stones - 4, ASTM, Philadelphia, PA.

ASTM D698-7. 1942. Standard Test Methods for Laboratory Compaction Characteristics of Soil Using Standard Effort. Annual Book of ASTM Standards, 04.08, Soil and Rock; Building Stones - 4, ASTM, Philadelphia, PA.

ASTM D854. 1945. Standard Test Methods for Specific Gravity of Soil Solids by Water Pycnometer. Annual Book of ASTM Standards, 04.08, Soil and Rock; Building Stones - 4, ASTM, Philadelphia, PA.

Barenblatt, G.I., Zheltov, I.P., and Kochina, I.N. 1960. Basic concepts in the theory of seepage of homogeneous liquids in fissured rocks. Journal of applied mathematics. 24, 1286-1303.

Blatz, J.A., Graham, J., and Chandler, N.A. 2002. Influence of suction on the strength and stiffness of compacted sand-bentonite. Canadian Geotechnical Journal. 39(5), 1005-1015.

Das, B. M. 2006. Principles of Geotechnical Engineering. Boston: PWS-Kent.

Delage, P. 2007. Microstructure features in the behaviour of engineered barriers for nuclear waste disposal. Experimental Unsaturated Soil Mechanics. 11-32. Weimar, Germany.: Springer Proceedings.

El Sohby, M.A., and Rabba, E. A. 1981. Some factors affecting swelling of clayey soils. Geotechnical Engineering Journal, SEAGS, 19 – 39.

Fredlund, D.G., Stone, J., Stianson, J. and Sedgwick, A. 2011. Determination of water storage and permeability functions for oil sands tailings. Proceedings Tailings and Mine Waste. Vancouver BC.

Fredlund, D. G., and Xin, A. 1994. Equations for the soil-water characteristic curve. Canadian Geotechnical Journal, 31, 521-532.

Fredlund, D. G., and Rahardjo, H. 1993. Soil mechanics for unsaturated soils. Canada: John Willey & Son.

Ito, H., & Komine, H. (2008). Dynamic compaction properties of bentonite-based materials. Engineering Geology, 98, 133–143.

Graham, J., Saadat, F., Gray, M.N., Dixon, D.A., and Zhang, Q.Y. 1989. Strength and volume change behaviour of a sand-bentonite mixture. Canadian Geotechnical Journal. 26(2), 292-305.

Gwo, J.P., Jardine, P.M., Wilson, G.V., and Yeh, G.T. 1995. A multiple-pore-region concept to modelling mass transfer in subsurface media. Journal of Hydrology. 164(1-4), 217-237.

Haverkamp, R. and Parlange, J.Y. 1982. Comments on: A physicoempirical model to predict the soil moisture characteristic from particle-size distribution and bulk density data. Soil Science Society of America Journal, 46, 1348-1349.

Juang, C.H., Holtz, R.D. 1986. A probabilistic permeability model and the pore size density function. International Journal for Numerical and Analytical Methods in Geomechanics. 10(5), 543-553.

Kleppe, J.H., and Olson, R.E. 1985. Desiccation cracking of soil barrier. In Hydraulic barriers in soil and rock. ASTM STP 874. Edited by A.I. Johnson, R.K. Frobel, N.J. Cavalli, and C.B. Pettersson. ASTM International, West Conshohocken, Pa. pp. 263–275.

Kraus, JF, C.H., Erikson, A.E., Chamberlain, E.J. 1997. Freeze-thaw cycling and hydraulic conductivity of bentonite barriers. Journal of Geotechnical Engineering. ASCE. 123(3), 229-238.

Kumar, S., and Yong, W. L. 2002. Effect of Bentonite on Compacted Clay Landfill Barriers. Journal of Soil and Sediment Contamination, 11(1), 71-89.

Mathew, P.K., and Rao, S.N. 1997. Influence of cations on compressibility behaviour of a marine clay. Technical Note, Journal of Geotechnical and Geoenviromental Engineering, ASCE,123 (11), 1071-1073.

Mingbin, H., Fredlund, D.G. and Fredlund, M.D. 2009. Estimation of SWCC from grain size distribution curves for loess soils in china. 62nd Canadian Geotechnical Conference Halifax, NS, Canada.

Mualem, Y. 1986. A new model for predicting the hydraulic conductivity of unsaturated porous media. Water Resources Research, 12, 513-522.

Romero, E., Hoffmann, C., Castellanos, E., Suriol, J., and Lloret, A. 2005. Microstructural changes of compacted bentonite induced by hydro-mechanical actions. In: Advances in Understanding Engineered Clay Barriers. (Eds) Alonso, E., Ledesma, A. 193-202. A. A. Balkema Publishers.

Romero, E., Gens, A., and Lloret, A. 1999. Water permeability, water retention and microstructure of unsaturated Boom clay. Engineering Geology. 54. 117-127.

Samper, J., Zheng, L., Montenegro, L., Fernandez, A.M., Rivas, P., and Dai, Z. 2005. Direct and inverse modelling of multicomponent reactive transport in single and dual porosity media. In: Advances in Understanding Engineered Clay Barriers. (Eds) Alonso, E., Ledesma, A. 493-504. A. A. Balkema Publishers.

SoilVision Systems Ltd (1999). User's guide for a knowledge-based database program for estimating soil properties of unsaturated soils for use in geotechnical engineering. Soil Vision Systems Ltd. Saskatoon, Saskatchewan, Canada.

Stewart, D.I., Studds, P. G. and Cousens, T.W. 2003. The factors controlling the engineering properties of bentonite-enhanced sand. Applied Clay Science, 23 (1–4), 97–110.

Tay, Y.Y., Stewart, D.I., and Cousens, T.W. 2001. Shrinkage and desiccation cracking in bentonite-sand landfill liners. Engineering Geology. 60(1-4), 263-274

Tien, Y.M., Wu, P.L., Chuang, W.S., and Wu, L.H. 2004. Micromechanical model for compaction characteristics of bentonite-sand mixtures. Applied Clay Science. 26(1-4), 489-498

Van Genuchten, M.T. 1980. A closed-form equation for predicting the hydraulic conductivity of unsaturated soils. Soil Science Society of America Journal, 44, 892–898.

Villar, M.V., and Lloret, A. 2008. Influence of dry density and water content on the swelling. Applied Clay Science, 39, 38–49.

Wersin, P., Johnson, L.H., and McKinley, I.G. 2007. Performance of the bentonite barrier at temperatures beyond 100 °C: a critical review. Physics and Chemistry of the Earth, 32, 780-788.

Wiebe, B., Graham, J., Tang, G.X., and Dixon, D. 1998. Influence of pressure, saturation, and temperature on the behaviour of unsaturated sand-bentonite. Canadian Geotechnical Journal. 35(2), 194-205.

Ye, M. W., Schaze, S., Qian, L. X., Wang, J., and Arifin, Y.F. 2007. Characteristics of swelling pressure of densely compacted Gaomiaozi bentonite GMZ01. Chinese Journal of Rock Mechanics and Engineering 26, 3861–3865 (in Chinese).

Highlights:

- At a clay content range, sand shape/sorting control the Sand-Bentonite properties
- **Sand-Bentonite mixtures are bi-modal thereby having structure-based properties**
- Informed design of sand fraction will limit the formation of desiccation cracks